Thermoelectric Power Production: Exploration of Applications with Concentrating Solar Arrays

David Kelly
Physics, BA; Mathematics, BA
University of North Carolina at Chapel Hill
kellyda@email.unc.edu

April 14,2014

Abstract

This study explores the many facets of a solar concentrated thermoelectric power system, and seeks to analyze their application. A simple solar thermoelectric system is designed and analyzed. Using a parabolic trough, solar radiation is focused directly onto thermoelectric devices, while a running water system is used to dissipate waste heat from the modules. A mathematical model is formulated to understand the relationship between absorbed power, hot side temperatures, and the efficiency of output power. Both controlled and raw outdoor experiments are carried out to explore the performance of the system. In controlled experiments the thermoelectric devices produce 110-130 mW of power, with efficiencies of 4-7%. Outdoor tests yield much more variable power, with average power production near 8 mW, and 0.5% efficiency.

Nomenclature

Symbol	Name	Value	Unit
α	Seebeck Coefficient		$\mu V/K$
δ	Earth Declination Angle		deg
$\dot{Q}_h$	Hotside heat Flow Rate		W
$\dot{Q}_h$	Rate of heat flow		W
η	Efficiency		$\%$
γ	Concentrator Facing Direction		deg
ω	Solar Hour angle		$deghour$
Ω	Solid angle		Sr
ϕ	Latitude		
π	Peltier Coefficient		W/A
ρ	Electrical Resistivity		Ωm
σ	Stefan-Boltzmann Constan	5.60373×10^{-8}	$Wm^{-2}K^{-4}$
τ	Thomson Coefficient		
θ	Angle between Aperture normal and Sun direction		deg
ε	Emissivity		
A_a	Collector Aperture Area		m^2
C	Specific Heat		J/K
D	Distance to heat source		mm
E	Seebeck EMF		V
G_SC	solar constant	1367	W/m^2
h	Convective heat transfer coefficient		W/m^2K
H_0	Horizontal Surface Radiation, no atmosphere		W/m^2
H_b	Direct Beam radiation		W/m^2
H_d	Diffuse sky radiation		W/m^2
H_g	Horizontal surface Radiation		W/m^2
k	Thermal conductivity		W/mK
K_T	Clearness index		
L	Plane wall thickness		m
M	Mass		kg
N_d	day number	$0 < 1 < 365$	
Nu	Nusselt Number		
q	Rate of heat flow		W
r_d	ground diffuse Reflectance		
Ra	Rayleigh Number		
T_{amb}	Ambient Temperature		K
T_c	Cold Side temperature		K
t_clock	Respective time of observer		
T_h	Hot side temperature		K

t_s	Solar time	
A	Cross Sectional area	m^2
a	Effective Width of TEG	mm
b	Effective Length ot TEG	mm
d	Parabolic Diameter	m
f	parabolic Focal length	m
h	Parabolic height	m
I	Current	A
I	Irradiance	W/m^2
l	Length of Parabolic Trough	m
n,m,N	Number	
P	Power	W
R	Resistance,Electrical	Ω
T	Temperature	K
V	Voltage	V

1 Introduction

In 1823, following the heyday of the industrial revolution, steam engines were the work horse machines of the time. With environmental and sustainability concerns almost certainly being non-existent, these machines operated at roughly 3% efficiency. Though this is not an astounding efficiency, and it certainly would not do by today's standards, these machines enabled and facilitated the industrial revolution. At this same time, however, Thomas Seebeck made an important discovery that could be the path to clean and efficient energy today. Seebeck observed that an electrical potential was built up when a junction of two different conductors was exposed to a temperature gradient. That is, he discovered an important property which can be used to convert thermal energy directly into electricity. Had he been able to combine some of the materials he was researching, he could have easily created a heat engine which was every bit as efficient as the steam engines of his time [15].

This alternative heat engine would not come into being for many years, though, due to Michael Faradays discovery of the connection between electromotive force and magnetic flux. Though Thomson and Peltier would later go on to make important discoveries relating to thermoelectric properties, these effects would remain relatively unstudied for decades. This lack of interest has left the thermoelectric generators of today at a relatively low efficiency in comparison to other electricity generators. However, unlike in Seebecks day, our power production methods today necessitate a high degree of environmental concern. As the need for clean and reliable energy resources increases, alternative production methods must be explored. Currently thermoelectric generators, while they are not incredibly efficient, have a promising future in various applications. The aim of this research, like many other current studies, is to explore a facet of those applications and assess the possibility of using these devices to capture and use naturally available energy.

1.1 Current Research

The thermoelectric effects (which will be described in the following sections) are the subject of a broad range of research topics. From system applications to materials research to the atomic-level physical interactions, the thermoelectric explorations are quite diverse. While the material research is an interesting topic, and certainly plays a role in the potential power production of TEGs, this study aims to examine the application aspects of these devices and is thus not entirely concerned with the current topics of materials research as they relate to the thermoelectric phenomena. A brief description of material properties will, however, be included in following sections.

There are several system applications for capturing energy with thermoelectric devices (similarly, there is a plethora of applications which use these devices as heat pumps, but those applications are outside of the scope of this paper). Current exploration of nuances and applications of the thermoelectric effects can be divided into two main categories: Direct power generation, and Cogeneration.

1.1.1 Direct Power Generation

One obvious use of thermoelectric devices is direct power production. To be specific, there are many applications in which thermoelectric devices could be used solely to produce electricity. As a matter of fact, the physical experiment that is the subject of this report is a direct power generation application. These direct power generation applications can be grouped as follows.

Synthetic Heat Sources
A simple application of TEG systems is to create some heat-releasing reaction, and use the TEGs to capture some of expelled energy. These include various thermo-chemical reactions (such as combustion or nuclear decay), which act as a energy resource for the TEG to produce electricity from. In fact, these synthetic heat sources are utilized in conjunction with thermoelectric devices largely in space applications. The mars rover Curiosity has an on board radioisotope thermoelectric generator to power its mission [10]. While space applications are very viable applications of thermoelectric technology with synthetic heat sources, the low efficiency of TEGs prevents them from being widely used with, say, combustion reactions because there are much more efficient means of capturing energy from these reactions currently.

Natural Heat Sources
As an alternative to synthetic heat sources, many scientists are exploring the use of TEGs in conjunction with natural heat sources. These sources can have a broad range in nature. From concentrated solar, solar ponds and even geothermal sources, there are many natural sources of energy which could provide renewable sources from which TEGs could draw their power [22, 17]. The aim of this report is to explore an application of this type.

Waste Heat Sources
A final category of direct power production, and possibly the most favorable application of current TEG technology, is the conversion of waste heat into electricity. Many, many processes produce waste heat. The combustion engine for example wastes 70% of the combustion energy in heat. Nearly all large scale power production is by means of thermal reactions. Thus, there is an inherent loss of energy. Many are researching how to effectively utilize TEG systems to capture this waste heat. Whether in capturing the energy lost to friction, or in increasing the overall efficiency of other power producing methods [8].

1.1.2 Cogeneration

A secondary use of thermoelectric generators is in a cogeneration setting. That is, both electricity and usable heat are produced. While this category is arguably similar to the previous category of recovering waste heat, it is necessarily a different subject. Here both heat and electricity are purposefully produced, while previously heat was an unwanted byproduct of electricity production. There are two methods of cogeneration with thermoelectric systems: Produce electricity first and heat second, or vise versa. These systems

offer an increased overall efficiency in use of captured energy, and present multifaceted approaches to solving energy needs.

Primary TEG Power, Secondary Heat
Here, energy is directed to a TEG array, and electricity is first produced. Then, the heat that is rejected from the TEGs is utilized as a source of heat. For example, one application being explored is using a concentrating solar system to collect heat for TEGs, then the rejected heat is used to heat residential water [16].

Primary Heat, Secondary TEG Power
In this case, energy captured first to act as a heat source, and then a TEG system is used to siphon off a fraction of that energy to produce electricity. For example, energy may be used to heat water, and then a TEG system is used to capture some of the thermal energy and convert it to electricity. This could see large use in situations in which water is heated beyond a common usable temperature. Here, TEGs could, by removing some of the thermal energy of the water, not only reduce the temperature of the water, but also produce electricity at the same time [14].

1.2 Purpose of Study and Hypothesis

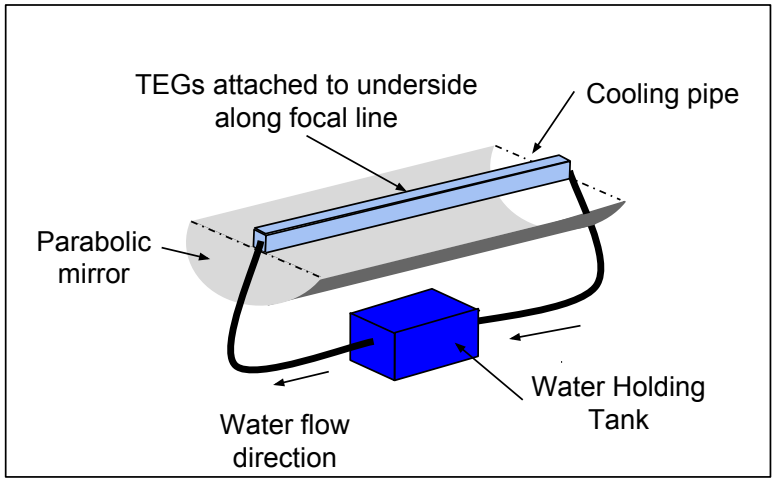

Figure 1: A square pipe with TEGs attached to the underside is oriented along the focal line of linear parabolic mirror. Water is pumped through the pipe to disburse the waste heat energy from the TEGs.

The aim of this research is to explore a facet of the renewable nature of thermoelectric applications. Specifically, a solar thermoelectric system is designed and analyzed. While previous research has indirectly transferred heat to the TEGs, systems like this stand to loose a great deal of power trough this transfer. Thus, this research will heat the devices

directly in an effort to reduce energy losses. Furthermore, a cooling system is necessarily required for thermoelectric power production. Given its availability and high specific heat, running water is used to dissipate the waste heat energy from the system. Thus, in theory focusing solar energy directly onto the face of thermoelectric devices, and by cooling them with a running water system, provides a system which is suitable for large scale power production.

To test this hypothesis, a system as in Figure 1 is used. A linear parabolic mirror is used to concentrate solar energy onto the face of three TEGs. Moreover, these devices are connected to what will be called the 'cooling assembly'. A square aluminum pipe provides a flat surface to which the TEGs are connected. Water is moved through this pipe to help dissipate the unused solar energy from the TEGs. A theoretical analysis will describe and quantify the potential electric output in this type of situation, and a physical experiment will be used to verify and further test these theoretical findings. These endeavors are specifically aimed to determine if a system such as this can be scaled to be used either in commercial power production, or to be used in a private residential situation. To begin, a brief description of current thermoelectric research is given.

2 Thermoelectric Properties and Theory

To begin to rigorously study and analyze the potential of the proposed system, it is important to understand the thermoelectric phenomena. It will be essential to first develop an understanding of the physical effects which enable thermoelectric power generation. Following this, a brief look into the thermal nature of these devices and the use of semiconductor materials will lead into a discussion of the power generation capabilities of thermoelectric devices. These developments will provide a strong physical basis from which the capabilities of the proposed system are built upon. To begin, the thermoelectric phenomena are described.

2.1 Thermoelectric Effects

There are three key effects which are generally presented on the subject: The Seebeck effect, the Peltier effect, and the Thomson Effect (each named for the scientist who first discovered them). Making use of the simple model in Figure 2, these effects are briefly defined here following Pollock's, Dechers and Joffes descriptions [13, 7, 5].

2.1.1 Seebeck Effect

The Seebeck effect is arguably the most important thermoelectric phenomenon. Indeed, as Pollock points out, the Peltier and Thomson effects are resultant and dependent upon the Seebeck effect [13]. The *absolute Seebeck effect* is observed in any conductor held in a temperature gradient. Here, if a conductor has its ends held at different temperatures, then an electrical potential will build up across the conductor. To qualitatively describe this effect, consider a long box with freely moving particles. If one end of this box is cooled

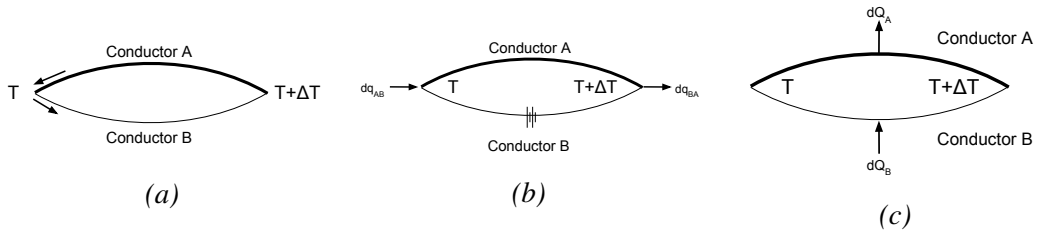

Figure 2: Thermodynamic circuit to explain Seebeck, Peltier and Thomson effects. Pollock's work [13].

and the other is heated, then the particles in the hot end of the box will gain more kinetic energy than those at the cool end. As such, these particles will begin to move around the box. Since the cool particles are relatively stagnant, the hot particles will tend to move to the cool end much more quickly than the cold particles move into the hot end of the box. Now suppose these particles are charge carriers. As the hot charge carriers move towards the cool end of the box, there will be a build up of charge at that end, resulting in an overall electrical potential across the box. This is as Teutsch states "a tendency for heat to drag along electricity" [19]. Furthermore, the *absolute Seebeck coefficient*, α, denotes the rate of change of this potential as it depends on temperature for a specific material. While an absolute Seebeck coefficient proves difficult to determine, a relative Seebeck coefficient is more easily found.

Consider Figure 2a. The absolute Seebeck effect dictates that an electrical potential will be generated in each of conductors A and B. Then, the relative difference between these two potentials produces an electromotive force (EMF) E_{AB} in the wire. This is called the *relative Seebeck EMF*. The rate of change in this EMF at a given temperature is the *relative Seebeck coefficient*, given by

$$\alpha_{AB} = \left[\frac{dE_{AB}}{dT}\right]_T$$

Thus it is clear that α is given in units of V/K. Specifically, the Seebeck coefficient for many thermoelectric generators are on the order of $200-300\ \ \mu V/K$. As will be shown in the following section, the thermodynamic nature of this relative EMF allows for the thermoelectric characterization of many materials.

2.1.2 Peltier Effect

Due to the resultant current that is produced by the relative Seebeck EMF, the *Peltier Effect* is the absorption or expulsion (reversible) of heat at the junction between two conductors. This is shown in Figure 2b with an external power source. As current flows across the boundary between two conductors, heat will either be given off or taken in at that junction. The *Peltier coefficient* π_{AB}, then, is the change in heat content Q at the junction between A and B as it relates to the current I,

$$\pi_{AB} = \frac{Q}{I}$$

This absorption and rejection of heat has found widespread use in cooling technologies. Peltier plates, as they are commonly called, can be found in diverse applications from water tanks to computers. Moreover, the reversible nature of Peltier effect gives rise to the heat engine qualities of thermoelectric generators.

2.1.3 Thomson Effect

Similar to the Peltier Effect, the *Thomson Effect* dictates that heat is evolved or absorbed as current passes through a single conductor in a temperature gradient, shown in Figure 2c. As current passes through a homogeneous wire whose ends are held at different temperatures, heat is given off or absorbed throughout the length of the wire. Therefore, the *Thomson coefficient* τ relates the heat dq given off (or taken in) by a wire to the current dI flowing through it and its imposed temperature gradient $\partial T/\partial x$ over a length dx as

$$dq = \tau dI \frac{\partial T}{\partial x} dx$$

Here it is important to note that this is very different from Joule heating. The Thomson effect is independent of the resistive qualities of the material, while Joule heating is related to the resistance of the conductor (it is often called 'resistive' heating). Furthermore, the Thomson effect is due to a temperature gradient imposed on the conductor to which Joule heating nominally has no relation. Moving forward, the thermal nature of the Thomson effect and the other thermoelectric effects are used to relate these three effects.

2.2 Thermodynamic Considerations

Continuing to use Figure 2, we can now consider the thermodynamic relationship between each of these three effects. Denoting the relative Seebeck EMF generated in this closed loop due to the temperature difference as E_{AB} the relative Seebeck coefficient is dE_{AB}/dT, and thus the electrical power is

$$IE_{AB} = I \frac{dE_{AB}}{dT} \Delta T$$

and thus, eliminating the common current term on each side

$$E_{AB} = \frac{dE_{AB}}{dT} \Delta T$$

Furthermore, the Peltier and Thomson Effects contribute to the net thermal energy of the system. The Peltier effect will contribute to energy absorbed and released at the junctions, while the Thomson effect will lead to a similar energy exchange in each of the conductors themselves. The balance of energy in this circuit mandates that the electrical power produced from this temperature gradient must be matched by the rejection and absorption of heat both at the junctions and across the two conductors [5], thus

$$\frac{dE_{AB}}{dT} = \pi_{AB}(T + \Delta T) - \pi_{AB}(T) + (\tau_B - \tau_A)\Delta T$$

Then, continuing to follow Pollock's derivation [13], dividing through by ΔT gives

$$\frac{dE_{AB}}{dT} = \frac{\pi_{AB}(T+\Delta T) - \pi_{AB}(T)}{\Delta T} + (\tau_B - \tau_A)$$

Letting ΔT approach zero, it is seen that

$$\frac{dE_{AB}}{dT}\Delta T = \frac{d\pi_{AB}}{dT} + \tau_B - \tau_A$$

Thus we have shown a fundamental linkage between the electrical potential (Seebeck effect) and the thermal potentials (Peltier and Thomson effects) of the thermoelectric phenomena. A distinct relationship between thermal characteristics (temperature) and electrical potential (E_{AB}) has been shown for a thermocouple as in Figure 2. This relationship is critical for the production of power from thermoelectric materials. Furthermore, relationships between each of α, τ and π can be shown through various entropy and conservation considerations [7]. With these relationships it is possible to describe the thermoelectric power production entirely in terms of the Seebeck coefficient α. Additionally, it is important to note that the relative Seebeck coefficient is independent of a flowing current. Thus, considering an open circuit, the relative Seebeck coefficient dE_{AB}/dT is given by

$$\frac{dE_{AB}}{dT} = \alpha_A - \alpha_B$$

where α_A and α_B are the absolute Seebeck coefficients of conductors A and B respectively. This fact presents a key quality which is utilized, in conjunction with the other thermodynamic relationships, to evaluate the thermoelectric effects in different materials. That is, given this equation, it is possible to build up a knowledge base of Seebeck coefficients for various materials.

The absolute Seebeck coefficient α then is directly related to electrical potential E_{AB} by means of a temperature gradient dT. Thus, for any two conductors there are a number of relationships that may exist between α for each material. Specifically, there are two extreme cases: either each of α_A and α_B increase at the same rate with temperature, or they diverge at exactly opposite rates with temperature. Generally, the latter case is unfavorable due to its non-linear nature. The former case is most desirable, and has lead to the widespread use of semiconductor technology in thermoelectric devices.

2.3 Power Generation

Simple inspection of the respective units of the Seebeck coefficient α (V/K) and the temperature gradient ΔT (K) lead one to see that the voltage across a load resistance as in Figure 3a is

$$V = \alpha \Delta T$$

Furthermore, because the p and n legs of a thermocouple are in series, the internal resistance of a single thermocouple is given by the sum of the resistance of each of these legs

$$R = R_p + R_n$$

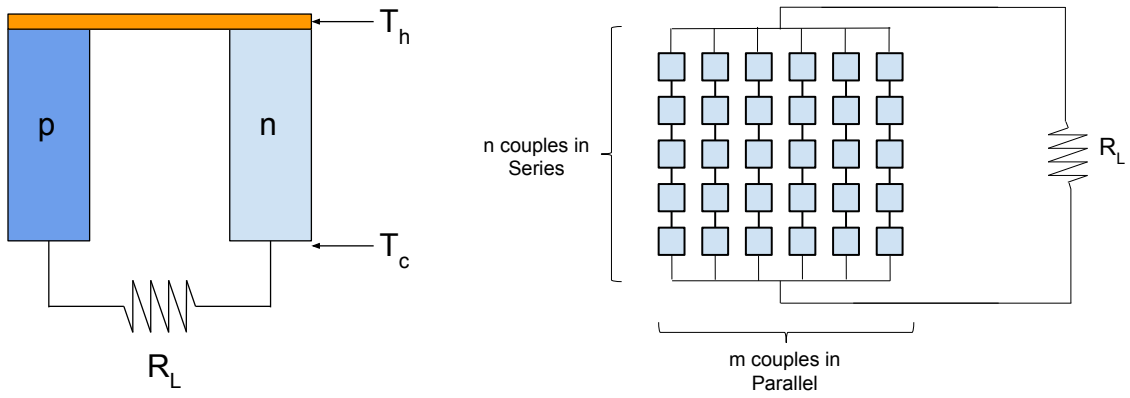

(a) *(b)*

Figure 3: (a) shows a single thermocouple made of p-type and n-type semiconductor materials in dark and light blue respectively. The two ends of the couple are held at T_h and T_c. (b) Diagram of thermoelectric generator with load resistance R_L. Here the blue squares represent each of the $n \times m$ total thermocouples.

Additionally, each p and n leg has its own electrical resistivity ρ_i. Thus, for legs of length L and cross sectional area A_i, the total internal resistance R of a single thermocouple is

$$R = \left(\rho_p \frac{A_p}{L}\right) + \left(\rho_n \frac{A_n}{L}\right)$$

Therefore, the current across the load resistance R_L is

$$I = \frac{\alpha \Delta T}{R + R_L} \tag{1}$$

Given a known temperature gradient (ΔT) and material parameters (α,R) it is straight forward to find the power output from a single couple. That is, using Ohm's law, the power output P in watts will be given by

$$P = I^2 R_L = \left(\frac{\alpha \Delta T}{R + R_L}\right)^2 R_L$$

However, power producing thermoelectric devices rarely will use a single couple. Referencing Figure 3b, first consider n thermocouples in series. The current across the load resistance is

$$I = \frac{n\alpha \Delta T}{R_{tot} + R_L}$$

Here, R_{tot} is the total internal resistance of the n thermocouples. Assuming that each thermocouple offers the same internal resistance R, then $R_{tot} = nR$. Furthermore, it is

typical to connect thermocouples in parallel to boost overall performance. Then, if there are m of these nR chains in parallel, then the internal resistance is given as

$$R_{tot} = \frac{1}{1/nR + 1/nR + \cdots + 1/nR} = \frac{1}{m/nR} = \frac{nR}{m}$$

The power output for a general thermoelectric device is

$$P = I^2 R_L = \left(\frac{nm\alpha\Delta T}{\frac{nR}{m} + R_L} \right)^2 R_L \tag{2}$$

Equation 2 will be especially useful in modeling and predicting the performance of the TEGs within the proposed system. Typically, the total internal resistance and the total number of couples in a device are listed. For a working version of Equation 2 we can let N be the total number of couples, and R be the total internal resistance, giving

$$P = \left(\frac{N\alpha\Delta T}{R + R_L} \right)^2 R_L \tag{3}$$

The ΔT term in this equation will lend this analysis easily to determining device performance and efficiency.

2.4 Efficiency

As with any system doing work, the efficiency of a TEG will be given by the ratio of useful work done to the input energy. In the case of this electrical system it is pertinent to look at the electrical power. Generally, the efficiency η is

$$\eta = \frac{P}{\dot{Q}_h}$$

where $\dot{Q}_h$, in units of watts, is the flow rate of heat onto the hot side of the device. By considering the reversible energy flowing through an element due to the Seebeck, Peltier and Thomson effects, as well as the irreversible energy flow due to resistive heating, Joffe [7] shows that

$$\dot{Q}_h = \alpha(T_h - T_c)I + K(T_h - T_c) - \frac{1}{2}I^2 R$$

where K is the total thermal conductivity of the device. The efficiency, then, using $P = I^2 R_L$, is given by

$$\eta = \frac{I^2 R_L}{\alpha(T_h - T_c)I + K(T_h - T_c) - \frac{1}{2}I^2 R}$$

where I is calculated by equation 1. Letting $m = R_L/R$ then the efficiency can be shown to follow Carnot efficiency as

$$\eta = \left(\frac{T_h - T_c}{T_h}\right) \times \frac{\frac{m}{m+1}}{1 + \frac{KR}{\alpha^2} \times \frac{m+1}{T_h} - \frac{1}{2}(T_h - T_c)\frac{1}{m+1}} \tag{4}$$

First, Equation 4 shows that the temperature difference $T_h - T_c$ across the device is critical for the overall efficiency. Being able to maintain this temperature gradient will facilitate higher efficiencies. Furthermore, the term $\frac{KR}{\alpha^2}$ captures all of the material properties of the device. The figure of merit Z is the inverse of this term and gives a measure of the electrical properties as they relate to the thermal properties in a material. For a thermocouple this is defined as

$$Z = \frac{(\alpha_p - \alpha_n)^2}{KR}$$

where α_p and α_n are the respective Seebeck coefficients for the p- and n-type elements. Using this term, the efficiency can be optimized for the ratio m. To find maximum efficiency as it relates to this ratio, we simply look for roots of the derivative of the efficiency as it relates to m

$$\frac{\partial \eta}{\partial m} = 0$$

Solving shows the optimal ratio of the internal to the external resistance $(R_L/R)_{opt}$, denoted as M, is

$$\left(\frac{R_L}{R}\right)_{opt} = M = \sqrt{1 + \frac{1}{2}Z(T_h - T_c)}$$

Then using this in Equation 4 we find

$$\eta = \left(\frac{T_h - T_c}{T_h}\right) \times \frac{M - 1}{M + \frac{T_c}{T_h}}$$

It is clear that if $M > 1$ then efficiency suffers. So there are two consequences. First, the load resistance needs to match the internal resistance. This is often called 'load matching', and will be a key topic in analyzing the performance of the proposed system. Second, M depends on Z. The desire is to match Z with a given application. Furthermore, Z shows that it is desirable to have materials with low thermal conductivity and a low internal resistance (or in other words, high electrical conductivity). While many metals have high electrical conductivities, they are also fairly good thermal conductors. Hence, thermoelectric devices often make use of semiconductor materials. The theory of these materials as they relate to thermoelectric devices is developed in the following section.

2.5 Thermoelectric Transport Theory

As has been discussed in the description of the thermoelectric effects, charge carriers in a material have a tendency to carry heat with them. This tendency not only gives rise to the thermoelectric effects, but it also contributes to the limiting factors of thermoelectric devices. In the previous section it was seen that an ideal thermocouple would be constructed

out of a material with a high electrical conductivity, and a low thermal conductivity. Thermal energy is carried through a material by either freely moving particles (electrons) or by waves passing through the lattice structure (phonon).

In a metal, the sea of electrons freely moves current with ease. However, these electrons also are the primary carriers of heat through the material. Thus the electrical and thermal conductivity of metals are intrinsically coupled to the movement of electrons through the material. Hence metals are not the usual choice of material for thermocouples because of the relative inability to increase electrical conductivity without also increasing thermal conductivity.

Semiconductors, on the other hand, have a slightly decoupled modes of heat and electricity transport through their material. Here, because the electrons do not readily form the same 'sea', phonons play a more significant role in the transfer of heat through the material. Thus, in essence, semiconductor materials are able to facilitate heat and electrical conduction via two different pathways. Because these pathways are now separate, if only slightly so, materials can be engineered so that thermal conductivity decreases while electrical conductivity increases. Therefore semiconductor materials are the ideal in creating thermocouples.

3 Solar Resource and Concentrating Methods

The sun's radiation will be the source of energy within this study. Accordingly, it is necessary to characterize this resource. To begin, the sun is commonly treated as a black body radiator. As such, it emits its energy (in the form of electromagnetic waves, or more simply, light) in all directions radially from its surface. Of particular interest is the light which is headed towards the earth. As this light travels across the cosmos it sees little impedance until it reaches the earth's atmosphere. Here the light is absorbed, reflected, or unhindered.

The NREL has compiled solar radiation data for various locations throughout the US over a 10 year span [11]. Taking Raleigh as a good approximation for Chapel Hill, concentrating solar devices see a daily average of 4.4 kWh$/m^2/$ solar radiation which is parallel to their parabolic axis. Given roughly 10 hours of sunlight in a day, this means that there is, at any given moment during the day, 4400 W$/m^2$ of usable solar radiation. This is a vast amount of power and capturing as much of that energy will be of primary concern.

Making use of this radiant energy is an interesting problem for which there are many solutions. One method is to concentrate the energy to a small location and use the resultant temperatures to do thermodynamic work. In order to maximize the total energy that can be used with such a method it will be important to not only understand the underlying concepts of concentrating collectors, but to also understand the movement of the sun.

3.1 Concentrating Collectors

Concentrating solar collectors are being used in wide spread renewable energy applications. By focusing solar radiation that would otherwise be falling on a relatively large area

to a small point or line, concentrating collectors are able to attain much higher temperatures, and do so with little to no input energy. There are several advantages associated with concentrating methods. First, because the sun's energy is focused to a small point, these collectors are able to attain relatively high temperatures. In fact, the Solana power plant project will be able to generate temperatures upwards of 380°C [12]. Second, the small area to which the radiation is focused helps to reduce convective losses. Furthermore, because reflective surfaces are generally far less expensive than absorbing surfaces [18], concentrators provide an economic advantage to non-concentrated methods. Therefore the renewable nature of this research is centered about the use of concentrated solar energy. What follows is a brief description of the concentrating geometry which will be used in this application, followed by a discussion on some of the limitations of concentrating methods.

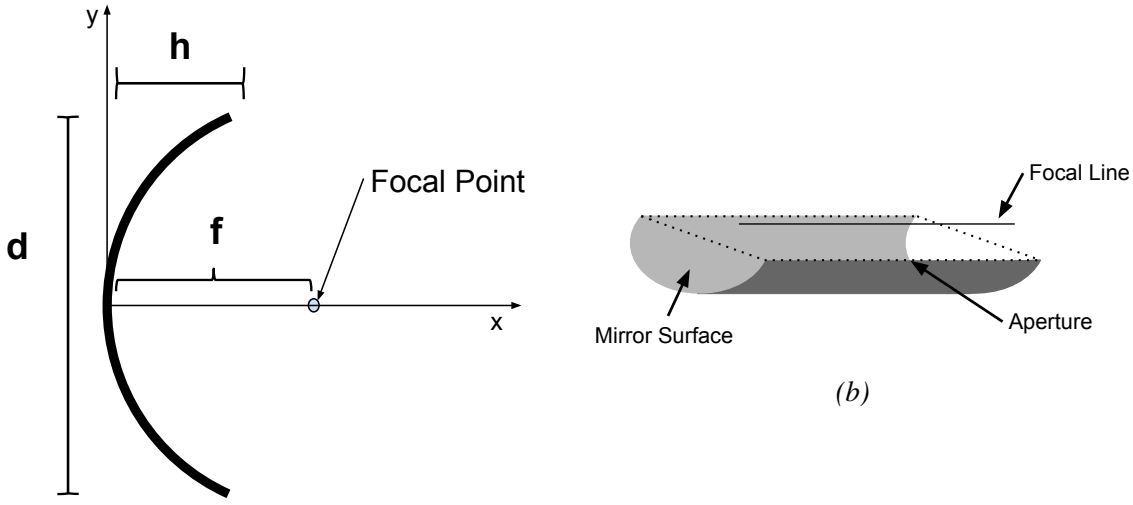

Figure 4: (a)Parabola and its dimensional variables, (b) Linearly translated parabola with its aperture and focal line pointed out

3.1.1 Solar Trough Geometry

A parabola is a fairly simple geometrical shape that acts as the backbone of concentration optics. The useful quality of the parabolic geometry is in its ability to re-direct light to a single point. That is, any beam of light which is parallel to the parabolic axis (the x-axis in the case of Figure 4a) is reflected to the focus point. To locate the focus point in terms of easily measured dimensions, an equation for a general parabola opening to the x-direction is

$$y^2 = 4fx \tag{5}$$

where f distance from the origin to the focal point. Using Figure 4a, then to relate the height of the parabola h to the focal length, we may set $y = d/2$ and $x = h$ in Equation 5 to find

$$h = \frac{d^2}{16f}$$

or, rearranging

$$f = \frac{d^2}{16h} \tag{6}$$

Therefore, Equation 6 gives the focus point of a parabola in terms of its height h and its aperture diameter d. These are easily measured for any parabola and thus provide a rather accessible calculation of the focus point.

If a parabola is translated along a line, the surface it forms is called a parabolic cylinder. More commonly this shape, shown in figure 4b, is referred to as a parabolic trough. Furthermore, this translation turns the focal point into a focal line. All light parallel to the parabolic axis that falls within the aperture of the trough will be directed to the focal line. For a trough of length l and parabolic diameter d, the area of the aperture A_a is given by

$$A_a = ld$$

Unlike a parabolic dish (where a parabola is rotated about its axis), which has only a focal point, the focal line of a solar trough is very adaptable to different systems. One such example is solar water heating. Here, a pipe is able to be positioned across the focal line, and water pumped through it. In a similar way a parabolic trough is used in this study to focus light onto a row of TEG devices, which are cooled by a pipe running across the parabolic trough. The linearity of the trough is ideal for flowing water systems.

3.1.2 Limitations of Concentrating Methods

Because a trough shape is open on its ends, it is possible that light will be reflected beyond the edge of the device. To be specific, if the source of light is on the left most side of the trough, then light which hits the right most side will be reflected even further to the right. This is often termed ‘end loss’. While it may not be a significant reduction in overall collected energy, it is a problem that is not present in parabolic dishes.

As mentioned in the previous section, a parabola is able to focus light which is parallel to its axis. While this is the alluring quality of a parabolic trough, it is also a very circumstantial. More specifically, the parabola is only able to focus light which is *parallel* to its axis. A parabolic mirror will not be able to make any significant use of light from any other direction. Therefore it is critical that the device point directly to the sun. The facing direction and tilt of the device will be critical in capitalizing on light rays that are parallel to the parabolic axis.

3.2 Device Tilt and Facing Direction

Concentrating solar devices are only able to make use of the light which is parallel to the normal axis of the aperture. These light rays are often termed ‘Direct’ or ‘Beam’. The

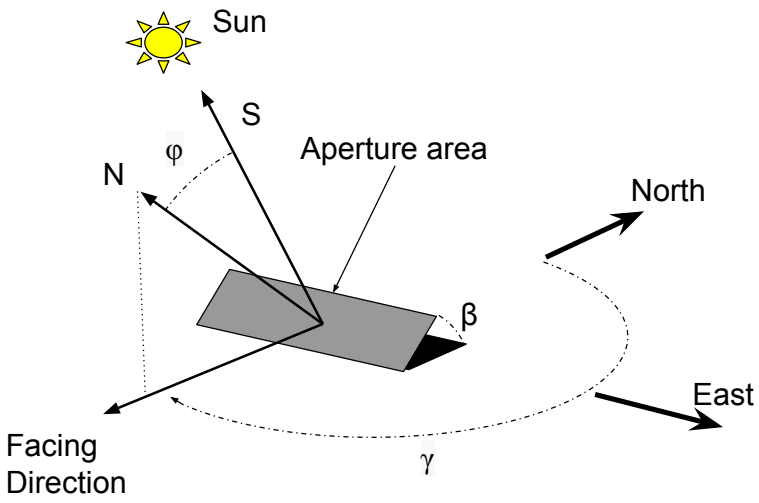

Figure 5: Various angles involved in determining proper tilt and facing direction for a solar collector.

irradiance that the aperture sees $I_{aperture}$ then will be given by

$$I_{aperture} = I_{sun} \cos \varphi$$

where φ is the angle between the normal vector of the aperture **N** and the unit vector pointing directly from the aperture to the sun **S** [18]. Referring to Figure 5, these angles may be seen more clearly. Therefore, it is desirable to adjust the array such that $\varphi = 0$. Pointing the device directly towards the sun is a simple concept, however it is the subject of rigorous astrophysics. To be brief, the daily spin of the earth, its rotation around the sun, and its seasonal declination angle δ, give a time varying (hourly, daily, seasonally) path of the sun which the device must track. Therefore, the optimum angle of tilt of the device β (measured from horizontal), and the ideal cardinal facing direction γ (measured from true North) will be dependent on position of the sun and the declination of the earth at a given moment. First, these parameters will be described briefly, then using an algorithm presented by Calabro [3] the optimum angle and direction can be determined for the device.

3.2.1 Solar Position

The earth's rotation is often described in terms of its hour angle ω. In effect the hour angle describes an observer's location in reference to the time when the sun reaches its highest point in the day. Technically, ω is the angle between the meridian of the observer, and the meridian which is directly in line with the sun. A meridian line is one which is drawn on the surface of the earth's sphere from the north pole through the equator and down to the south pole (i.e. longitude lines). The hour angle is defined in terms of the solar time t_s by

$$\omega = 15(t_s - 12)$$

It is important to note that the solar time is not quite the same as the standard clock time. Specifically, solar time is a 24 hour system in which 12:00 corresponds to the time when the sun is directly south of an observer (for an observer in the northern hemisphere). Thus the solar time will vary based on the day of the year N_d (out of 365 days). A general equation for the solar time is given by

$$t_s = t_{clock} + (0.258\cos x - 7.416\sin x - 3.648\cos 2x - 9.228\sin 2x$$

where

$$x = \frac{360(N_d - 1)}{365.242}$$

3.2.2 Earth's Declination Angle

While students learn early on in their education that the earth revolves around the sun, it often goes unmentioned that the earth 'wobbles' along this path. During spring the northern hemisphere leans towards the sun, while in the winter the the earth is leaning away from the sun. This lean will certainly have an effect on the observed path of the sun across the sky. The declination angle of the earth δ is defined as the angle between the equatorial plane and the line drawn from the center of the earth to the sun. An approximate equation to give δ in terms of the day number N_d is

$$\sin\delta = 0.339795\cos(0.98563(N_d - 173)) \tag{7}$$

3.2.3 Cardinal Facing Direction

A final parameter of importance is the cardinal direction which the array faces. Measuring from North, with clockwise angels being positive, γ will be used to describe the facing direction of the aperture. To be specific, γ is the angle between true North and the projection of the normal line of the aperture onto the horizontal plane. It is rather difficult to define the facing direction when the aperture is perfectly horizontal. However, as discussed earlier, it is not typical or ideal to hold a collecting surface at a zero tilt.

Typically for the Northern Hemisphere a solar collection array is pointed due South, $\gamma = 180^\circ$. Noting that this is obviously not ideal as the sun moves across the sky during the day (rising in the east, setting in the west), it still serves as a good fixed tracking direction. Because the sun is nearly always in a southern direction for an observer in the northern hemisphere, it will suffice to hold the direction of a solar collector facing south. There are indeed gains to be made, however, with a system that tracks the sun in all directions. That said, the specific application will mandate the degree of sophistication of the tracking system. In the case of a solar trough the cardinal direction need not track throughout a single day as the array can be pointed such that the sun's path follows the focal line of the device.

3.2.4 Determining Ideal Angles

Finding the ideal angle to tilt a solar collector is a rather complicated issue, as has been prefaced in the previous sections. However, there are simplified and fairly straight forward approaches to determining the proper angle. One such algorithm is outlined here based on Calabro's work [3]. First, there are a few terms which need to be defined. The daily radiation on a horizontal surface without the effects of an atmosphere is H_0. This can be approximated by

$$H_0 = 86400\frac{G_{SC}}{\pi} \times \left(1 + 0.033\cos\left(2\pi\frac{N_d}{356}\right)\right)\cos\phi\cos\delta \times \left(\pm\sqrt{1-\tan^2\phi\tan^2\delta}\right) + \cos^{-1}(-\tan\phi\tan\delta) \times \sin\phi\sin\delta \quad (8)$$

where $G_{SC} = 1367 \ \ Watts/m^2$ is the solar constant, N_d is the day number, δ is the solar declination and ϕ is the latitude of the device.

Furthermore, a clearness index K_T can relate this radiation to the daily radiation on a horizontal surface H_g (in the presence of an atmosphere), by

$$K_T = \frac{H_g}{H_0}$$

Note that H_g is an observed radiation and is easily found in published data tables [11]. This global horizontal radiation is made up of a horizontal diffuse sky irradiation H_d and a direct beam irradiation H_b. The clearness index is also related to H_d by

$$\frac{H_d}{H_g} = 1.35 - 1.61K_T$$

Then, using H_0, H_d, H_g, and the diffuse reflectance of the ground ρ_d, the ideal tilt angle from horizontal β, and cardinal direction γ can be determined for a specific sun angle ω.

$$\beta = \tan^{-}1\left\{H_0 \times (\cos\delta\sin\phi\cos\omega\cos\gamma - \sin\delta\cos\phi\cos\gamma + \cos\delta\sin\gamma\omega) \times \left[\left(H_0 + \frac{H_d}{2} - \frac{H_g\rho_d}{2}\right) \times (\sin\delta\sin\phi + \cos\delta\cos\phi\cos\omega\right]^{-1}\right\} \quad (9)$$

$$\gamma = \tan^{-1}\left\{\frac{\cos\delta\sin\omega}{\cos\delta\sin\phi\cos\omega - \sin\delta\cos\phi}\right\} \quad (10)$$

Therefore, in a straight forward fashion one can calculate find the ideal tilt angle and cardinal direction given these formulas developed here. Given radiation data (H_g, r_d), and the time, one can easily find the proper tilt angle β.

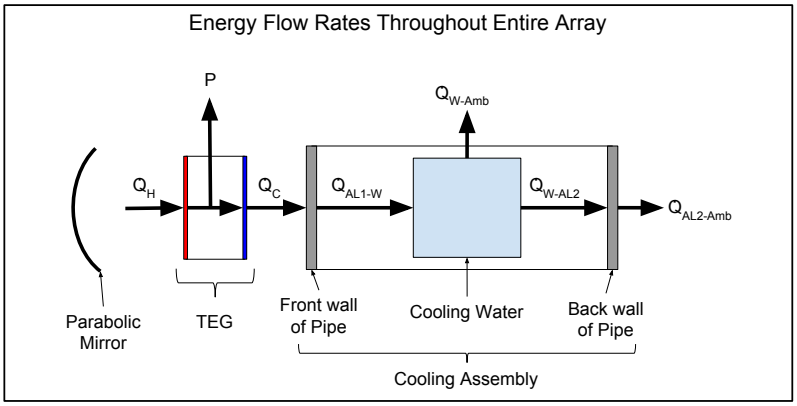

Figure 6: Energy Flow Rates through out entire array. Theses rates are related to the thermal properties of the materials and will be described in the following sections

4 Thermal Considerations

The thermal properties of this system will be the critical factors in determining the overall power output of the array. Therefore, it is important to consider the ways in which heat energy moves through the system. Specifically, we wish to see how energy will enter the system, how it will leave the system, and the net gain of energy for each piece in the system (here 'piece' will refer either to the cooling pipe, water in the pipe, or the water in the holding tank). The power production of the TEG is dependent on the hot and cold side temperatures, thus this analysis is primarily concerned with understanding the factors that affect these temperatures. Many of the thermal properties involved in such a system are described here, and some will be used in later sections to analyze and predict the performance of the system.

4.1 Energy Entering System

Solar Energy will be radiated onto the face of the devices through the mirror surface (or in the case of controlled experiments, directly from the heat source). Here we develop an understanding of quantifying radiation energy. Radiation sources will be treated at black body radiators. The Stefan-Boltzman law states that the total energy radiated per unit surface area j^* of a black body is directly proportional to the fourth power of the its temperature T

$$j^* = \sigma T^4$$

Where $\sigma = 5.670373 \times 10^{-8}$ W$/m^2K^4$ is the Stefan-Boltzmann constant. This same principal may be used in the case of reflection. However, if a body absorbs part of its incident radiation, then the power radiated from its surface will be

$$j^* = \varepsilon \sigma T^4$$

where ε is the object's emissivity and is less than one. Then in terms of the total power P radiated form the object the equation becomes

$$P = Aj^* = A\varepsilon\sigma T^4$$

Where A is the unit area area which receives the radiation. Rearranging, then will give the power in W/m^2, P/A, as

$$\frac{P}{A} = \varepsilon\sigma T^4 \tag{11}$$

The conservation of energy mandates that the power radiated from a source P will be equal to the difference between the power radiant on the hot side of the TEGs P_h and the power radiated to the ambient P_{amb}.

$$P = P_h - P_{amb}$$

Applying Equation 11 gives

$$\frac{P}{A} = \varepsilon\sigma\left(T_h^4 - T_{amb}^4\right) \tag{12}$$

where T_h and T_{amb} are the hot side temperature and ambient temperatures respectively. Thus we have developed an equation to describe the heat P radiated from a body.

4.2 Transfer of Energy Within the System

Figure 6 shows a broad overview of the energy transfers within the system at any given instant. The main focus will be on the transfer of energy from the cold side of the TEG to and through the cooling assembly. Since these pieces are in direct contact, the energy will move via conduction. In general the rate of heat diffusing across a plane wall is

$$q = \frac{T_1 - T_2}{\Theta} \tag{13}$$

where T_1 and T_2 are the temperatures on the face of either side of the wall. The thermal resistance Θ is given by

$$\Theta = \frac{L}{KA}$$

with L being the thickness of the wall, A being the cross sectional area perpendicular to the direction of heat flow, and K being the thermal conductivity of the wall material in $watts/mK$. Specifically, this equation will be used to find the energy conducted from or to the aluminum piping.

Lastly, each piece of the cooling assembly will gain energy. This will inherently lead to an increase in temperature. The change in temperature of each piece can be related to the instantaneous energy it gains dQ by

$$dQ = MC(T_f - T_i) \tag{14}$$

where M is the mass of the piece, C is its specific heat, and T_f and T_i are the finial and initial temperatures, respectively. This will be used for all pieces of the cooling assembly.

4.3 Dissipation of Energy Away from the System

Continuing to refer to 6, it is clear that energy will exit the system via convection. For a body at a given temperature the rate of heat convection is

$$q = h(T - T_{amb}) \tag{15}$$

where T is the temperature of the piece and T_{amb} is the ambient air temperature. The convective heat transfer coefficient h is a rather complicated function of the cross sectional area, the width, and any surrounding conditions about the piece. A more simplistic approach will be necessary in this situation. Here it is useful to first consider the Nusselt number Nu. This dimensionless term gives the ratio of the convective heat transfer to the conductive heat transfer at the boundary of a material

$$Nu = \frac{hL}{K}$$

Thus if Nu is near 1, the conduction and convection processes are near equal in magnitude. For large values of Nu the convection far outweighs the conduction. Therefore, if the Nusselt number is known for a particular situation, then given the width L and thermal conductivity K of the piece, the convective heat transfer coefficient can be found by

$$h = \frac{NuK}{L} \tag{16}$$

However, the Nusselt number is not so easily determined analytically. To simplify matters an average Nu will be used. In the case of free convection from a horizontal plate, Nu is given by [21]

$$Nu = .54Ra^{1/4}$$

where the Rayleigh number Ra is the dimensionless number corresponding to free convection. For the horizontal plate, Rafalls between 10^4 and 10^7, which gives $8.5 < Nu < 48.2$ for this situation in particular.

5 Experimental Setup

5.1 Description

A square aluminum cooling pipe is oriented across the focal line of a parabolic trough. Three thermoelectric devices are fastened with mounting collars to the pipe such that the focal line lies directly across the devices. A pump connected to a DC power supply is used to circulate water (the cooling fluid in this experiment) through the pipe. Figure 1 in the beginning of this report gave a broad view of this experimental set up, while Figure 7 gives a more detailed view, including the sensor arrangements.

Hot side temperatures are be measured via a temperature sensor placed along the focal line of the mirror, just as the TEGs. This measurement is critical to determine and

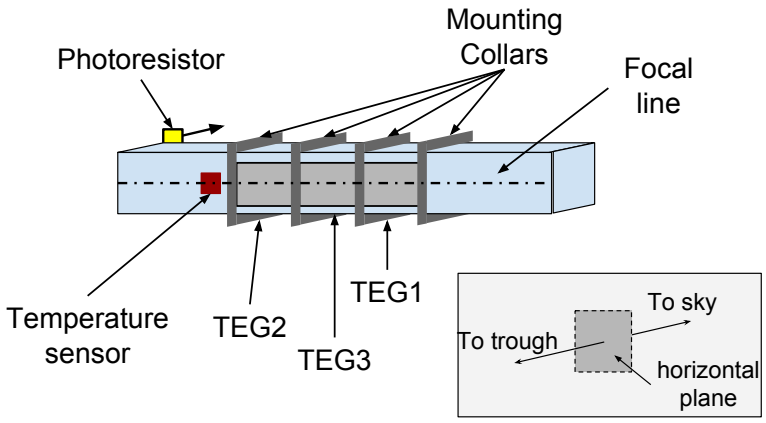

Figure 7: Underside view of sensor and device placement in experimental set up. Note that TEG3 is nested between TEGs 1 and 2.

understand the efficiency of the devices. Furthermore, a photoresistor pointed upwards to the sky is used to give an indication of possible factors (amount of cloud cover) which decrease overall power production. Experimental data is recorded autonomously via a micro controller system. Specifically, analog measurements from the temperature sensor, photo resistor, and voltage measurements from each TEG across its own load resistance are recorded.

Before delving into experimental analyses, it is worthwhile to discuss the selection and justification of this system at hand.

5.2 System Justification

Since the desire here is to explore the renewable nature of thermoelectric devices, an obvious source of energy is solar. Hence, a concentrated solar collector is used. Although concentrated solar power is able attain higher temperatures than otherwise possible, it does so passively. Consequently, the hot side temperatures are largely outside of the control of the designer. The designer does, however, have control of the dissipation of the waste heat from the system. Essentially, the dissipation of heat is made easier by indirectly heating the devices. While many researchers prefer to heat the devices indirectly, this system heats the devices directly in an attempt to minimize thermal losses associated with indirect methods. Directly heating the devices in this way requires an immediate cooling system which does not drastically impinge on the energy collected. A solar trough is used here because its linear nature nicely facilitates the use of a running water system to cool the devices.

Furthermore, a solar trough offers a significant ability to be scaled to large size that is often cumbersome for dish-type solar concentrators. Similarly, using water as a cooling system is also lucrative for a potentially large power facility. First, the remarkably high specific heat of water enables it to absorb a large amount of the waste heat. Additionally, water is for all intents and purposes readily accessible, making it the common cooling fluid

of choice for many applications. The availability and strength of water make it the clear choice in many cooling situations.

5.3 Equipment

In order to thoroughly explain the experiment, a brief description of the equipment used is given. Herein an approximation of associated measurement error will be also be given. The relevant equipment and parameters are tabulated at the end of this section.

Three 30mm by 30mm power generating thermoelectric devices were used. Specifically, CustomThermoelectric's 126 couple power generating devices were chosen not only for their reported power output, but also for the completeness of their reference data. Having access to a complete and thorough data set for these devices will be very useful in evaluating the overall system performance.

The thermoelectric devices were fastened to an aluminum square pipe with aluminum collars. Shims were used to secure the collars in place. Aluminum was chosen for the cooling assembly because of its high thermal conductivity. The purpose of the cooling assembly was to dissipate the waste heat from the cold side to the TEG as quickly and effectively as possible. Thus, aluminum's high thermal conductivity made it the near perfect material for this purpose.

The parabolic mirror was sourced from a previous project, and provided an accessible structure to base this experiment. A polished stainless steel mirror made the reflecting surface for the parabolic trough. Furthermore, the previous project also provided a low power pump and water hold tank. Parameters for these devices are listed in the following table.

A TMP36 temperature sensor was used to measure the hot side temperatures. This sensor poses the limiting source of error in all measurements for this experiment, with an error of $\pm 1.5°$C. Furthermore, a photo resistor was pointed along the axis of the trough towards the sky. This sensor, though it did not give particularly quantitative data, it gave a qualitative measure of the radiation which the array is collecting. Specifically, it was used to account for the weather (clouds) conditions and their effect on the power production.

An Arduino Uno (a rather popular micro controller) was used to continuously and automatically record information about the experiment. For the outdoor experiments the output voltage of each TEG as well as the measurement data from the sensors was measured and recorded every two minutes. Bench top measurements were taken every two seconds. Using this micro controller enabled automatic and consistent data measurement.

5.4 Data measurement methods

Since the power output of the thermoelectric devices is most visibly related to the hot and cold side temperatures, measurements at these locations will be critical in evaluating the performance of the device. Therefore, a temperature sensor is positioned directly on the focal line on the face of one of the TEGs. Though this sensor will impede the energy flowing into that particular TEG, it is very important to have a measurement directly at the

Table 2: Equipment Specifications

Thermoelectric Generators	Value	Unit
Length	0.03	m
Width	0.03	m
Thermal Conductivity	1.75	$watts/mK$
Thermocouples	126	
Seebeck coefficient	2.01	$\mu V/K$

Aluminum Piping	Value	Unit
length	1.22	m
Width (outside)	0.0381	m
Width (inside)	0.035	m
Density	2.7	g/cm^3
Specific Heat	0.9	J/gK
Thermal conductivity	200	$watts/mK$

Water and Hold Tank	Value	Unit
Hold tank length	0.4	m
Hold tank width	0.3	m
Hold tank height	0.092	m

face of the device. This will of course lead to a reduction in the overall output of this TEG, however power from the other two modules will be unhindered.

Because the TEG modules are affixed directly to the face of the aluminum pipe, it is difficult to place one of the (rather thick) temperature sensors directly on the cold side of one of the TEGs without significantly reducing its thermal contact with the cooling pipe. Though it will not give an entirely accurate reading, the second temperature sensor will be placed on the side of the piping. This is a sacrifice in accuracy of measured data, but other recorded information (such as the output voltage) will be telling of the accuracy of this measurement.

As discussed earlier, the TEGs will produce a maximum power output under load matched conditions. Therefore, to match the internal resistance of the devices, a load of 5-6 Ω is required. During testing it is not readily possible to vary the load resistance of each device according to its current internal resistance. As such, two of the TEGs will operate under a 5Ω load, while the third will have a 6Ω load.

6 Experimental Analysis

To provide a thorough analysis of the performance of this system three analyses were carried out. First, a theoretical model was formulated and numerically iterated to provide insight for very idealized system properties. Next, controlled bench top tests were per-

formed to characterize the behavior of the cooling system. Finally, outdoor experiments were conducted to give an indication of the true performance of the system.

6.1 Modeling Theoretical Performance

6.1.1 Model Formulation

A simplified approach is taken to model the performance of this system. Treating the TEG as a lumped block of material we may use the heat equation to describe the temperature T with respect to location in the block x as

$$\frac{\partial T}{\partial t} = \frac{K}{\rho c_p}\frac{\partial^2 T}{\partial x^2} + \frac{q_v}{\rho c_p} \tag{17}$$

Where K,ρ,c_p give the thermal conductivity, density, and specific heat of the TEG block of material. Normally, q_v is the heat generated in the material per unit volume. However, we can instead impose that this term represent the electric power produced by the device. Recall that the electric power generated by the device P_{elec} is

$$P_{elec} = R_L I^2 = R_L \left(\frac{mS\Delta T}{R+R_L}\right)^2$$

Here, with the block positioned with its hot face at $x = 0$ and its cold face at $x = L$, then $\Delta T = T(0) - T(L)$ where L is the length of the TEG block. While there is some error involved, the respectively low temperature applications being explored here allow us to safely assume material parameters K, ρ, c_p, S are constant. Setting

$$\alpha = R_L \left(\frac{mS}{R+R_L}\right)^2$$

then we see that

$$q_v = \frac{-\alpha}{AL}\left(T(0) - T(L)\right)^2$$

Since we are primarily concerned with the steady state behavior of the system, Equation 17 gives

$$\frac{\partial^2 T}{\partial x^2} = \frac{\alpha}{AL}\left(T(0) - T(L)\right)^2 \tag{18}$$

To a good approximation we can say that the temperature at the end of the device will be equal to the temperature of the water,

$$T(L) = T_w$$

Additionally, we can impose a boundary condition on the front face of the device. The flux Φ (power per unit area) across this boundary will be proportional to the first derivative of the temperature with respect to position, evaluated at $x = 0$. That is,

$$-K\left.\frac{\partial T}{\partial x}\right|_{x=0} = \Phi$$

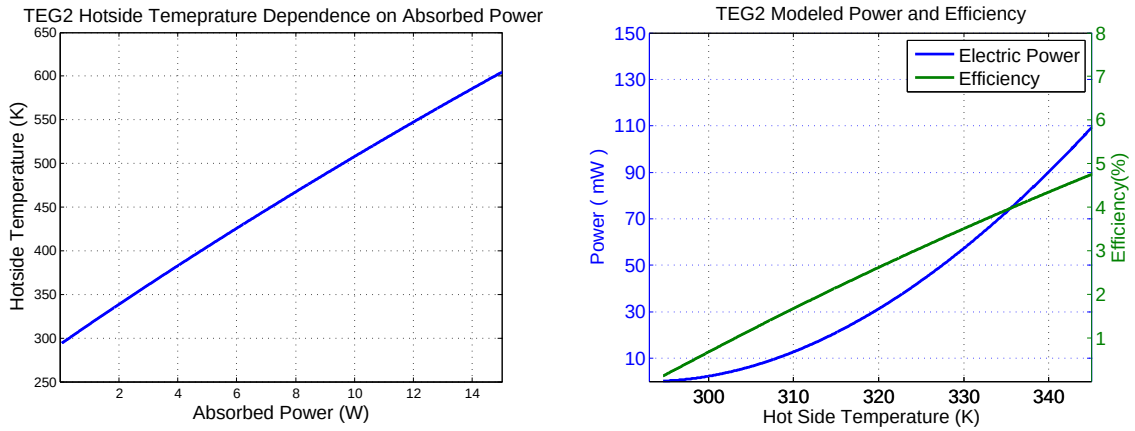

(a) *(b)*

Figure 8: Model Results for TEG2. (a) shows the near-linear relationship between absorbed power and hot side temperatures. (b) gives the output power on the left and efficiency on the right axis for various hot side temperatures.

The flux across the front boundary is given by

$$\Phi = \frac{1}{A}(P_{abs} - P_{rad})$$

where P_{abs} and P_{rad} give the absorbed and radiated heat in watts. The absorbed heat will be taken as a constant and will be given the by the power radiated from the mirror surface. The power radiated from the surface of the TEG, on the other hand, is given by

$$P_{rad} = \varepsilon\sigma AT(0)^4$$

as discussed in previous sections. Generally, since Equation 18 is a second order, ordinary differential equation the solution will have the form

$$T(x) = C_1x^2 + C_2x + C_3$$

Thus, given these boundary conditions, material parameters, and values for T_w and P_{abs} it is very straight forward to find the coefficients C_1, C_2, C_3.

6.1.2 Results

As preliminary results, Figure 8 shows the relationships between temperature and electric power for TEG2 (Similar figures for TEG 1 and 3 are included in the appendix). While these figures will later serve as a source of understanding for the operating efficiency of the system, they do present an estimate of the potential efficiency. Here the efficiency of the system is on the order of 5%. It would appear as though a simple method to increase the power output and efficiency of the system is to simply increase the temperature (by a larger concentrating surface, for example). However, the trend shown here is not necessarily true

at higher temperatures. This model has been formulated by assuming that the material parameters of the devices remain constant, which is certainly not true at high temperatures. With this in mind, we can use these model results to interpret experimental data.

6.2 Bench top Tests

In order to understand the ultimate efficiency of the cooling system, a series of bench-top tests are required. The thermoelectric devices were supplied with a constant source of heat. Accordingly, the output electrical power of each device was measured for varying water flow rates. These varied flow rates, as discussed in previous sections, directly affect the ability of the system to dissipate cold side waste heat from the devices.

6.2.1 Configuration

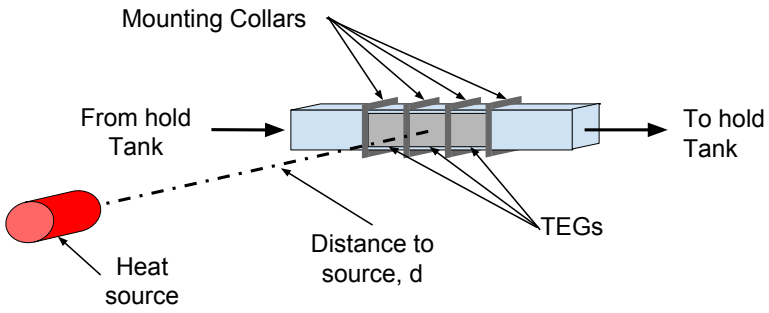

Figure 9: Diagram of bench top testing arrangement to analyze cooling system performance

Referring to Figure 9, a heat gun with a 2.54 cm diameter nozzle was used as a controlled and consistent heat source by which the nature of the cooling system could be analyzed. The device was pointed such that the normal line from the nozzle pointed directly in line with the normal of the TEGs along the cooling assembly wall. Using $18°C$ cooling water, the device was positioned 30 mm away from each thermoelectric generator separately. For each generator, voltage measurements are recorded at 2 second intervals for 5 minutes at three possible flow rates.

6.2.2 Radiant Power Calculation

In order to calculate the power incident on the TEGs in this set up, we first treat the heat gun as a blackbody radiator. Then, the emitted power from this source P_s is

$$P_s = A_s \sigma (T_s^4)$$

where T_s and A_s are the source temperature and surface area respectively. The heat q in watts that is radiated onto the surface of the TEG is given by [6] as

$$q = P_s \cos(\theta) \Omega$$

The angle between the normal line of the source and that of the receiving surface θ in this case is zero. Furthermore, Ω gives a measure of the relative size of the receiving surface in relation to its distance from the source. In other words Ω is the solid angle subtended by the receiving surface. In the case of a rectangular receiving surface, the solid angle can be calculated as [9]

$$\Omega = 4\arccos\left(\sqrt{\frac{1+C_a^2+C_b 2}{(1+C_a^2)(1+C_b^2)}}\right)$$

where C_a and C_b relate the length a and width b of the receiving surface to its distance D from the source

$$C_a = \frac{a}{2D}\ ,\ C_b = \frac{b}{2D}$$

The load resistance, relative length and width dimensions, calculated input power and the modeled output power for each device are are listed in Table 3. Specifically, the modeled output power here will help to validate the theoretical model of the system. Validation of the model will be critical for interpreting outdoor measurements.

Table 3: TEG calculated absorbed power and model predicted output power

	Load Resistance(Ω)	a (mm)	b (mm)	Input Power (Watts)	Output Power (mW)
TEG1	6.96	25.1	30	2.002	78.5
TEG2	4.84	26.1	30	2.071	89.8
TEG3	4.74	24.1	30	1.934	78.1

6.2.3 Results

Table 4: Measured electrical power output for various cooling fluid mass flow rates

Flow Rate (g/s)	Power, mW (Efficiency, %)		
	TEG1	TEG2	TEG3
287	106.4 (5.31)	92.6 (4.47)	130.8 (6.77)
340	110.3 (5.51)	93.4 (4.51)	130.3 (6.74)
400	108.3 (5.41)	94.1 (4.55)	129.4 (6.69)

At the onset, one would expect TEG3 and TEG2 to produce near equal power due to their similar load resistances. However, this is not the case. As Figure 10 shows, TEG3 produces much more power than either of the other two devices. This is likely due to the fact that TEG3 is positioned between the others. Being placed in this way, it is possible that the nested device is able to dissipate some of its waste heat to the devices on its perimeter, thus increasing its overall performance.

Furthermore, Figure 10 is ultimately descriptive of the cooling system performance. Recall that TEG1 and TEG2 have load resistances of 6.96 Ω and 4.84 Ω, respectively. As discussed in previous sections, a thermoelectric generator is most effective when working

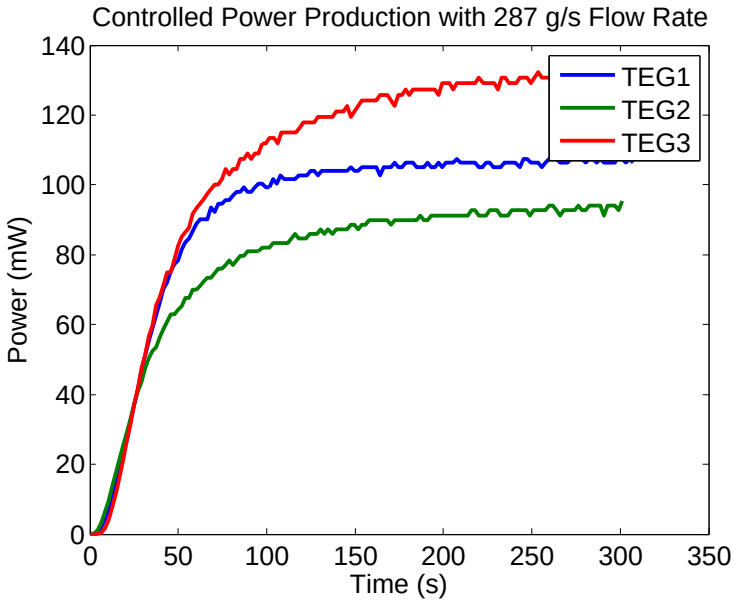

Figure 10: Controlled experiment with consistent heat source. 18°C water, moving at 0.287 kg/s, is used in the cooling assembly. Electrical power produced across loads of 6.96 Ω, 4.84 Ω, and 4.74 Ω for TEGs 1, 2 and 3 respectively

under a load resistance which matches its own internal resistance. Here, it seems as though the larger load resistance is better suited for the situation. Because the internal resistance of the device increases with its average temperature, and assuming that the hot sides of each of these devices in nearly the same, then we see that the back side of the devices are not especially cool. However, the cooling assembly does present a unique facet which is critical for power production.

Referring to Table 4, the effects of the flow rate on performance become more noticeable. While TEG1 outdoes TEG2 in all cases, each device sees a peak in its own production at different flow rates. TEG1 produces its most power (and most efficiency) with a cooling fluid flow rate of 340 g/s while TEG2 peaks at 400 g/s. This difference is evidence that the flow rate of the cooling fluid will change the average temperature of the device. Since TEG1 has a larger load resistance it will produce power more effectively when it is hot enough to have its internal resistance match this load. Thus, TEG1 peaks in performance at a slower flow rate. On the other hand, because TEG2 has a smaller load resistance, it requires a lower average device temperature in order to optimally match its respective load, which is achieved by means of a faster flow rate. Here it is clear that this proposed system has the ability to dynamically match its load. Additional figures showing power production for other flow rates can be found in the appendix (Figure 18).

Referring to 3, we see that TEG2 performs most similarly to the modeled predictions, with results varying only by roughly 4 mW from the model. This deviation is ultimately due to the simplifying assumptions made in formulating the model. It was assumed that the temperature at the back face of the device would be equal to the temperature of the water,

and that the temperature of the water would remain constant. While the water temperature for these experiments did not change dramatically throughout the testing process, however it is clear by 4 that the flow rate of the water has changed the relative back side temperature of the devices. The modeled predictions for TEG1 disagree greatly, and is likely due to the much larger load resistance of the device. TEG3, as discussed above, likely saw an additional effect of absorbed heat that was unaccounted for in the model. Thus, given these caveats, we can make use of the model predictions for the outdoor experiments.

6.3 Outdoor Tests

Several outdoor experiments, using actual solar radiation as the source energy, were carried out. These results give an implication of the working efficiency of this proposed system. Although the previous section has demonstrated the abilities of the cooling system, it is important to analyze the system holistically in order to understand issues which will affect the overall performance. Three key outdoor data sets were collected with the intention of exploring the performance of the system under different settings. For the first two tests data was collected for a two hour span at two different water flow rates. The final test used chilled cooling water in order to examine some extreme potential of the device.

It should be noted that these tests were performed in optimal conditions. These tests were only carried out on particularly sunny days. However, the ambient air temperature, as well as other factors like wind, contribute to non-static results. Although they were not explicitly used in this analysis, photoresistor and focal point temperatures were recorded. This data is presented in Figures 19 -24 in the appendix. They show the degree of variability in the solar resource even on a fairly clear, sunny day.

6.3.1 Data Collection

In order to observe the long-term results of this system, data was read and recorded from the sensors and TEGs every two minutes. Because of the dynamic nature of the weather, instantaneous readings would vary over time. Thus, taking readings every two minutes demonstrated aggregate behaviors of the system without a cumbersome dataset. In other words, it was unnecessary to see the near instant changes in performance for such a system. What was necessary, however, was data collected over a longer period of time. Here, these experiments were carried out for at least 1 hour, and 2 hours in most cases. These long experiments allow the system to reach, or at least approach, a working steady state.

6.3.2 Incident Power and Efficiency

Keeping in mind that the model predictions are generally very low for TEGs 1 and 3, and that they are fairly accurate for TEG2, we can make use of the model to extrapolate the absorbed power of the devices. That is, given measured output powers, we can approximate the efficiency of the system based on the model information presented in figures like 8b. Specifically, Figures13-17 in the appendix are used for their corresponding applications to approximate the operating efficiency of the devices.

6.3.3 Results

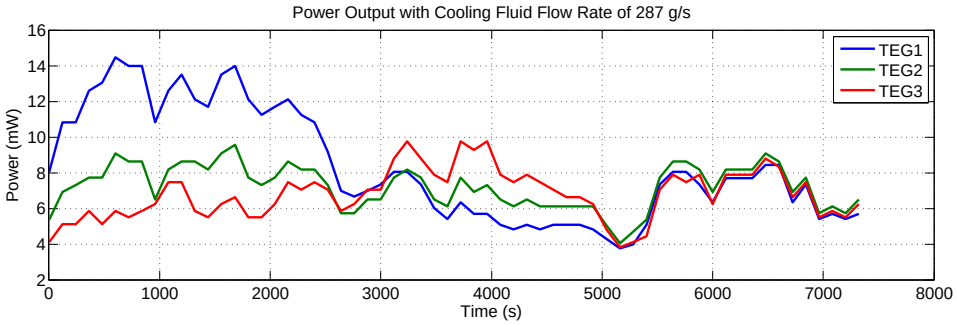

(a)

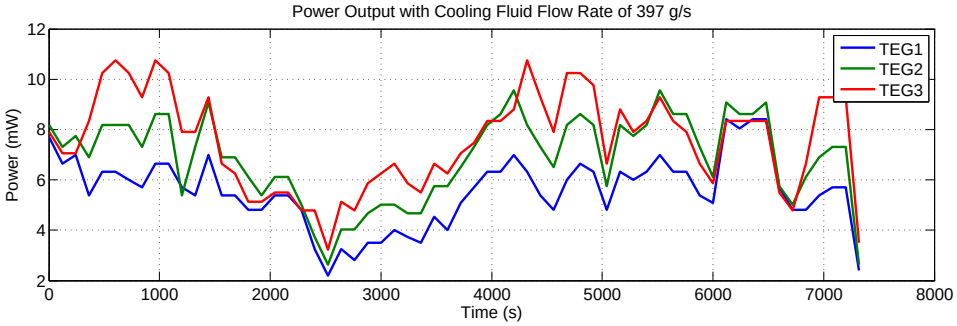

(b)

Figure 11: Two hour spans of data taken on a sunny and windy day. (a) Represents data taken with a 281 g/s cooling fluid flow rate, while data in (b) was measured with a 397 g/s flow rate.

Figure 11 gives the recorded output power for each device with two different cooling fluid flow rates. As was discussed in previous sections, notice that TEGs 2 and 3 outperform, generally speaking, TEG1 with the faster flow rate. In order to understand the potential of this system in dynamic (real world) conditions, we may look at the upper and lower bounds of power produced.

With a flow rate of 281 g/s, Figure 11a, shows that the power is found almost entirely between 4 and 14 mW. Furthermore the average power produced, across all three TEGs is 7.4 mW per device. While the standard deviation of this data is quite large (2 mW), we see that each device produces between 9.4 and 5.4 mW on average. Additionally, given the formulated model, we can approximate the efficiency of this system. Recall that the model presented a relationship between the output power, efficiency and hot side temperature of a device (as in Figure 8b). Based on these model calculations, each device was operated on the order of 0.5% throughout this experiment.

In Figure 11b, with a flow rate of 397 g/s the output power as a whole is lower than before. With a maximum power of nearly 10 mW, the faster flow rate, in general, has apparently given a lower overall power production. Here the average power produced is 6.6 mW, again with a standard deviation of 2 mW. Thus, the normal power output, in general, of a device in this operation is between 8.7 and 4.4 mW. This is a similar, but

slightly lower production in comparison to the faster flow rate. Here again the devices operate, by the model formulations, on the order of 0.5%.

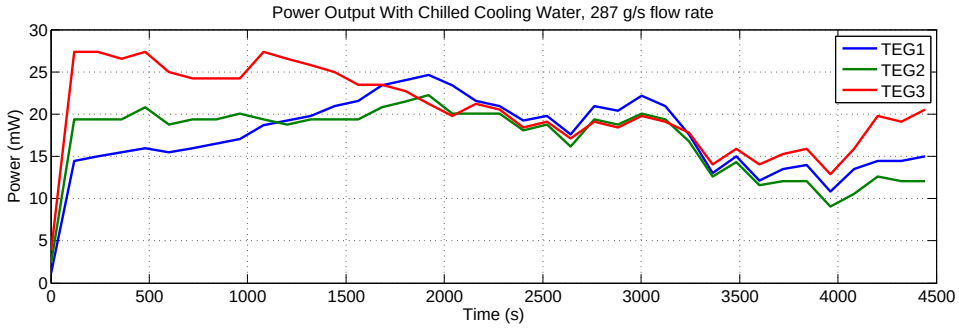

Figure 12: One hour span of data recorded on sunny, calm day with iced water cooling fluid flowing at 297 g/s

In order to explore the potential of this system, an experiment is carried out with ice water as the cooling fluid. In Figure 12 we see that the output is bounded between 10 and 28 mW. On average each device produces between 13.3 and 23.3 mW of power. Based on the model formulations, these devices were normally then operated at roughly 2.5% efficiency.

7 Study Implications and Conclusions

A simple solar concentrating thermoelectric system has been proposed and analyzed. It was supposed that the simplified approach of focusing solar energy directly onto the face of the devices, and cooling them via a moving water system would create a suitable power generation method. A mathematical model was formulated to predict and interpret power outputs for various conditions. Controlled bench top experiments were carried out to not only gage the effectiveness of this model, but also to explore the behavior of the cooing system. First, it was found that the model sufficed, generally speaking, to predict the output power of the devices. Second, the controlled experiments exemplified the effects of flow rate on power output which the model was not able to capture. Most importantly, we saw that larger flow rates were more effective for devices with larger load resistances. Controlled experiments showed efficiencies of 4-7%, while producing 105-130 mW of power for each device. Finally, outdoor experiments were carried out to examine the raw ability of this system. Using the formulated model to infer the working efficiency of the devices, the system was seen to operate at roughly 0.5% efficiency while producing approximately 4-9 mW of power per device.

Here the controlled experiments show a fair level of performance. Supposing the devices are able to produce 120 mW per second for 8 hours of sunlight, then each 30×30 mm device is able to produce 1Wh of power a day. Thus we quickly see the ability of a larger system. As a simple calculation, assume a system is constructed with 150 devices. Such an array would be approximately 4.5m long; a fairly small system. Assuming that

ideal power could only be produced in the 4 warmest months out of the year (June,July, August, September for North Carolina), then this array would produce 18kWh of power in that time. Alone this power seems fairly significant. However, according [4] , the average person in North Carolina consumed 14,325 kWh of electricity in 2010. Even this relatively small array that we have supposed would cost nearly $4500 for the TEGs alone. With power rates at $0.0967 per kWh, a person would only save approximately $2 on his or her energy bill for those 4 months. At this rate the costs far outweigh the benefits, at least financially. Moreover, the raw outdoor data found in this study even further reduce the viability of this system. However, with increasing demand for renewable energy sources, the capability of thermoelectric systems is not to be dismissed.

While this study has shown relatively low efficiencies and power outputs, especially for raw outdoor experiments, there are fairly simple adaptations that can be made to improve performance. First, a glass enclosure could be implemented to prevent convective losses to the ambient air. This enclosure would also circumvent any adverse effects caused by windy conditions. Additionally, a selective surface material on the face of the TEGs could be utilized to more efficiently absorb the most energetic wavelengths of light. Lastly, the mounting collars used in this research may have blocked too much incident radiation from the devices. Instead, an alternative mounting method could be used. For example, it may be more beneficial to sandwich the devices between the cooling assembly and a thermally conductive material. Light would then be focused onto the material first, then the heat would be transferred to the TEGs. All together, these measures present interesting cases for further research on this simple system.

Perhaps most interestingly this research has demonstrated the ability of this system in the context of a larger power system. Specifically, it was seen that the mass flow rate of the cooling fluid would match most efficiently to specific load resistances. Thus, such a system could easily be made to meet the dynamic load resistance of a real power grid very efficiently by simply adjusting the fluid flow rate. Although the specific optimal adjustment parameters would need to be studied, this research has demonstrated the ability of this system to achieve maximum efficiency for dynamic loads.

This research has presented many of the facets involved in a thermoelectric system. While it was proposed that this simple array could produce significant power levels, experimental measurements did not necessarily support that hypothesis. While the extreme case experiment (ice water) showed heightened performance, and while controlled experiments showed relatively high levels of efficiency, the power produced is still far too little for such a system to act as a viable power generation system. However, encouraging methods to improve this system have been proposed. All told, the passive nature of thermoelectric devices is very promising for renewable systems.

References

[1] Anjaneyulu, Y. *Energy Resources: Utilization and Technologies* BS Publications, Hyderabad, India. 2012.

[2] Bhandari, C.M.. *Thermoelectric Transport Theory*. CRC Handbook of Thermoelectrics. Edited by D.M. Rowe. CRC Press 1995.

[3] Calabro, Emanuele. *An Algorithm to Determine Optimum Tilt Angle of a Solar Panel from Global Horizontal Solar Radiation*. Journal of Renewable Energy. Volume 2013, Article ID 307547. 2013.

[4] California Energy Comission. *U.S. Per Capita Electricity Use by State in 2010.* Energy Almanac.

[5] Decher, Reiner, *Direct Energy Conversion: Fundamentals of Electric Power Production*. Oxford University Press, 1997.

[6] Incropera, DeWitt, Bergman, Lavine. *Fundamentals of Heat and Mass Transfer*. Wiley and Sons. 2007.

[7] Joffe, A.F., *Semiconductor Thermoelements and Thermoelectric Cooling*. Infosearch Limited, London, 1957.

[8] Lubieniecki, Michal; Uhl, Tadeusz, *Thermoelectric Energy Harvester: Design considerations for a bearing node* Journal of Intelligent Material Systems and Structures. 2012.

[9] Mathar, Richard J. *Solid Angle of a Rectangular Plate*. Max-Planck Institute of Astronomy. February 21, 2014. http://www.mpia-hd.mpg.de/ mathar/public/mathar20051002.pdf

[10] NASA, *Multi-Mission Radioisotope Thermoelectric Generator*, Space Radioisotope Power Systems. NASA. January 2008.

[11] National Renewable Energy Laboratories, *Solar Radiation Data Manual for Flat-Plate and Concentrating Collectors*.http://rredc.nrel.gov/solar/pubs/redbook/PDFs/NC.PDF

[12] National Renewable Energy Labratories, *Solana Generating Station* Concentrating Power Projects. 2013.

[13] Pollock, Daniel D. *General Principles and Theoretical Considerations*. CRC Handbook of Thermoelectrics. Edited by D.M. Rowe. CRC Press 1995.

[14] Rowe, D.M; Min, G., *"Simbiotic" application of thermoelectric conversion for fluit preheating/ power generation*. Energy Conversion and Management. V43 N 2, pp 221-228. 2002.

[15] Rowe, D.M. *Introduction* CRC Handbook of Thermoelectrics. Edited by D.M. Rowe. CRC Press 1995.

[16] Shakouri, Ali; Yazawa, Kazuaki, *Scalable Cost/ Performance Analysis for Thermoelectric Waste heat Recovery Systems*. Journal of Electronic Materials. V 41 N 6, pp 1845-1850. 2012.

[17] Stevens, James W. *Heat Transfer and Thermoelectric Design Considerations for a Ground-Source Thermoelectric Generator*. 18th International Conference of Thermoelectrics 1999.

[18] Stine, Geyer. *Power From the Sun* Online Resource. Adapted from *Solar Energy Systems Design* by Stine and Harrigan. 2001.

[19] Teutsch, Werner B, *Some Considerations of the Basic Physics of Thermoelectric Effects*. In *Thermoelectricity*. Edited by Egli, Paul H. 1960

[20] TXL Group, *Ultra-Low Voltage Bootstrap Converter* ELC-W0422-1/2 Datasheet. Custom Thermoelectric LLC. 2012.

[21] University of Pensylvania, School of Engineering and Applied Science. *Correlations List: External Free Convection Correlations*. http://www.seas.upenn.edu/ meam333/correlation/CorrelationsList.pdf 2013.

[22] Wu, C. *Performance of Solar-pond Thermoelectric Generators*. International Journal of Ambient Energy, V16 N 2, pp. 59-66. 1995.

Appendix Figures

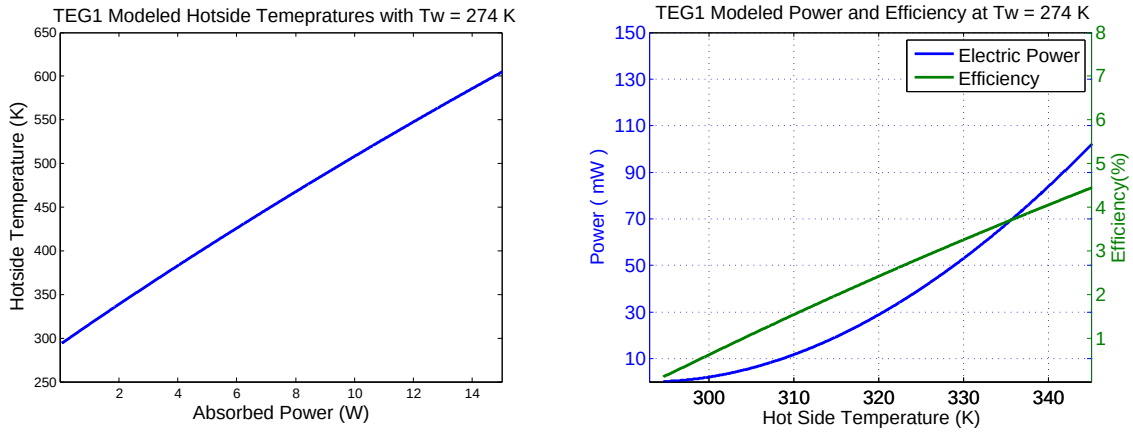

(a) *(b)*

Figure 13: Model Results for TEG1 with 293 K cooling water. (a) shows the relationship between absorbed power and hot side temperatures. (b) gives the output power on the left and efficiency on the right axis for various hot side temperatures.

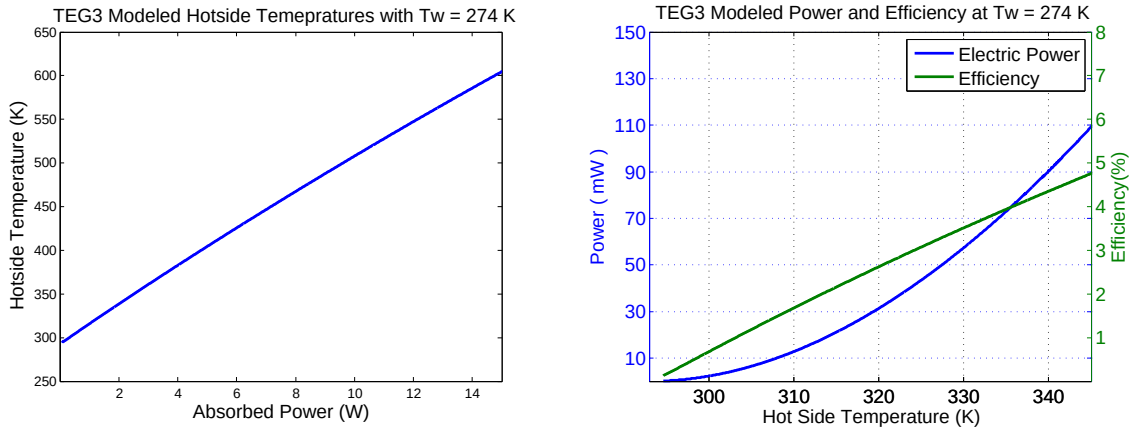

(a) *(b)*

Figure 14: Model Results for TEG3 with 293 K cooling water. (a) shows the relationship between absorbed power and hot side temperatures. (b) gives the output power on the left and efficiency on the right axis for various hot side temperatures.

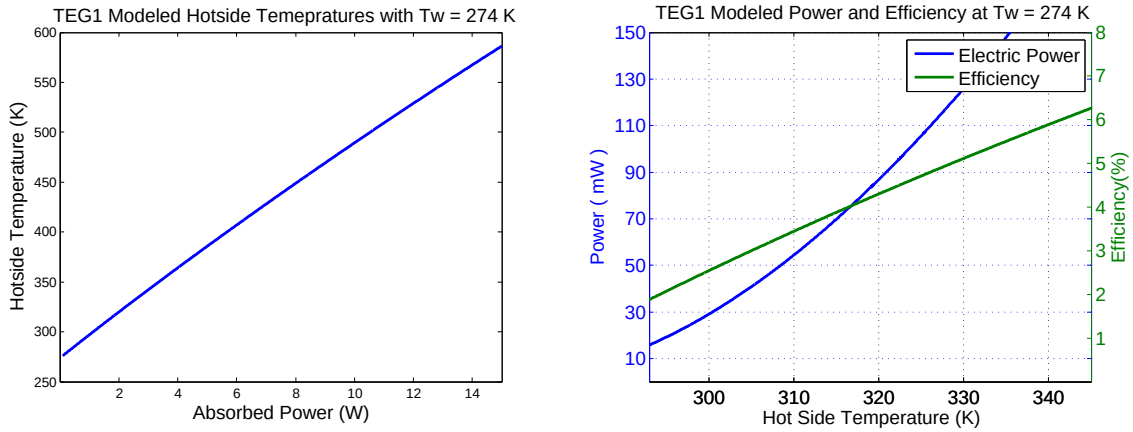

(a) *(b)*

Figure 15: Model Results for TEG1 with 274 K cooling water. (a) shows the relationship between absorbed power and hot side temperatures. (b) gives the output power on the left and efficiency on the right axis for various hot side temperatures.

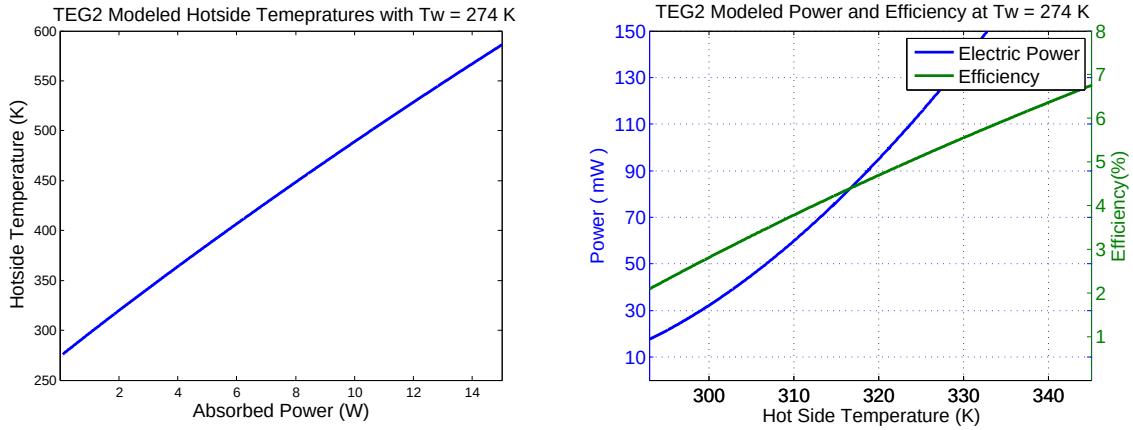

(a) *(b)*

Figure 16: Model Results for TEG2 with 274 K cooling water. (a) shows the relationship between absorbed power and hot side temperatures. (b) gives the output power on the left and efficiency on the right axis for various hot side temperatures.

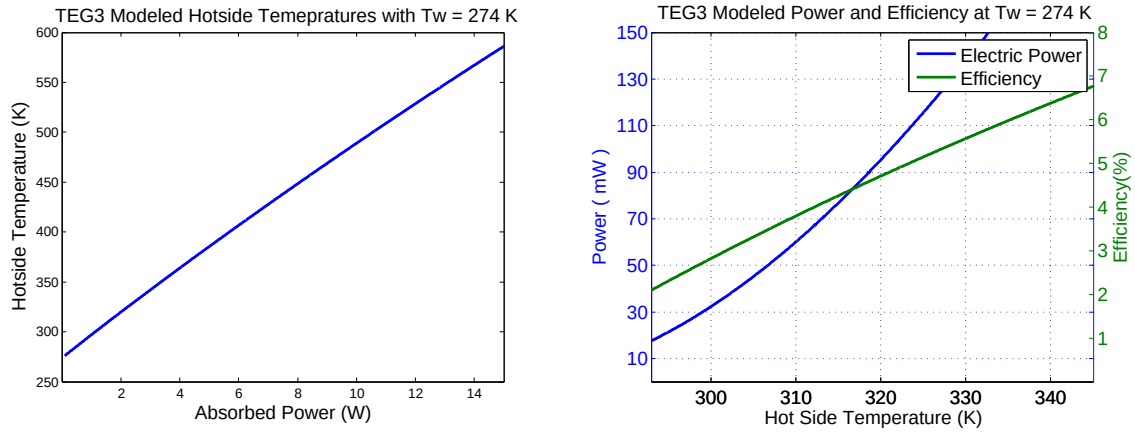

(a) *(b)*

Figure 17: Model Results for TEG3 with 274 K cooling water. (a) shows the relationship between absorbed power and hot side temperatures. (b) gives the output power on the left and efficiency on the right axis for various hot side temperatures.

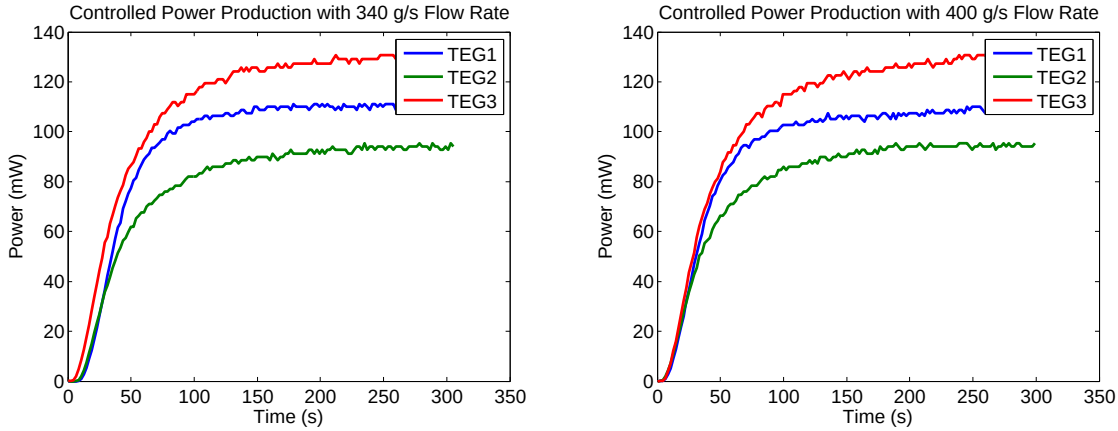

(a) *(b)*

Figure 18: Controlled experiments with consistent heat source 30 mm from the faces of the devices. 18°C cooling water moving at (a)340 g/s and (b) 400 g/s is used.

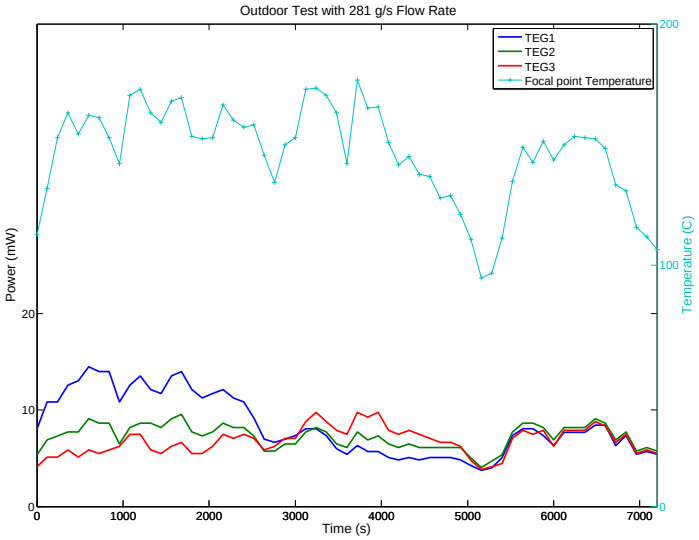

Figure 19: Power Measurements and recorded focal point temperatures for outdoor tests with cooling fluid flow rate of 281 g/s

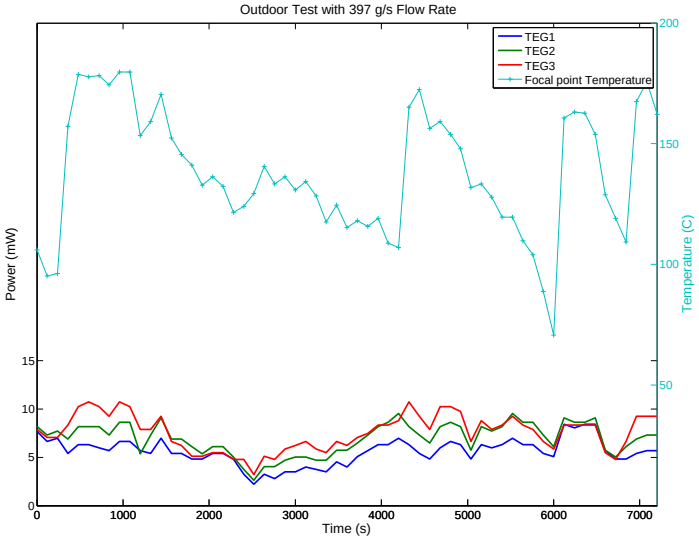

Figure 20: Power Measurements and recorded focal point temperatures for outdoor tests with cooling fluid flow rate of 397 g/s

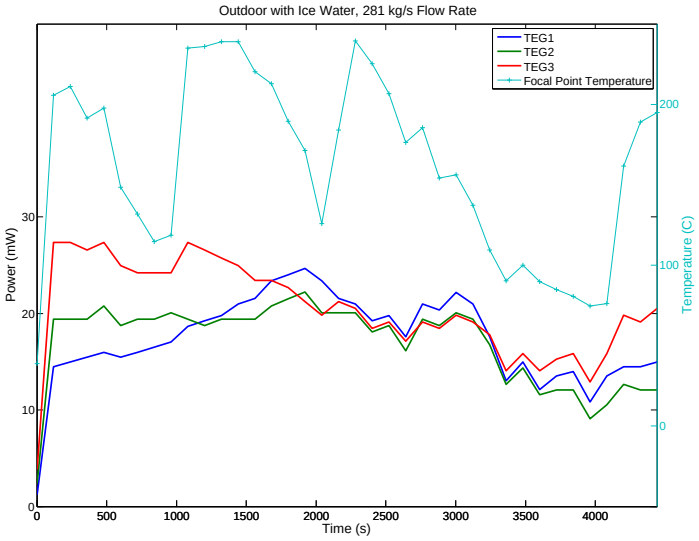

Figure 21: Power Measurements and recorded focal point temperatures for outdoor tests with Iced water with fluid flow rate of 281 g/s

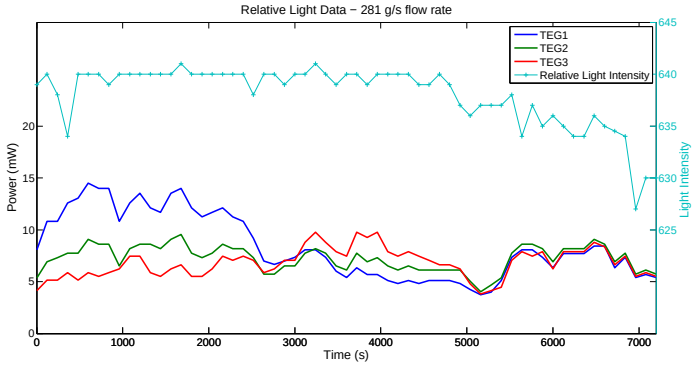

Figure 22: Measured Light data for two hour span of outdoor experiments taken with cooling fluid flow rate of 281 g/s.

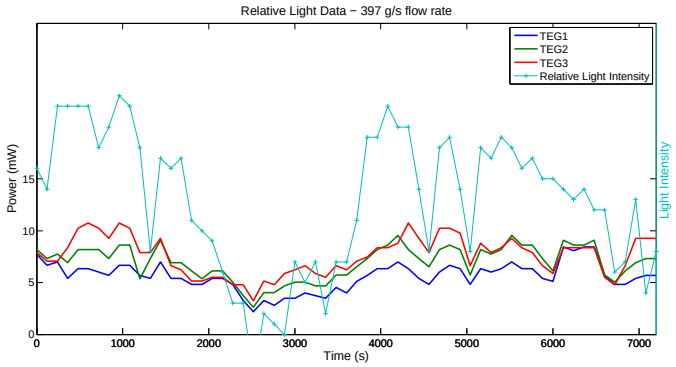

Figure 23: Measured Light data for two hour span of outdoor experiments taken with cooling fluid flow rate of 397 g/s.

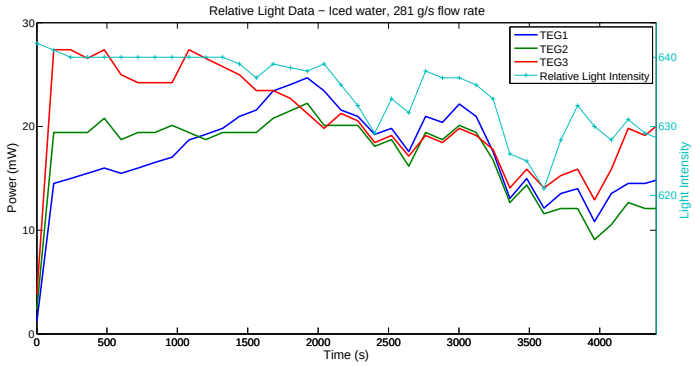

Figure 24: Measured Light data for 1 hour span of outdoor experiments with iced cooling at a flow rate of 281 g/s.